ELSEVIER

Journal of Nuclear Materials 317 (2003) 117–129

journal of nuclear materials

www.elsevier.com/locate/jnucmat

# Determination of dislocation density and composition of β-Zr in Zr–2.5Nb pressure tubes using X-ray and TEM

Young Suk Kim *, Sung Soo Kim, Yong Moo Cheong, Kyung Soo Im

*Zirconium Group, Korea Atomic Energy Research Institute, P.O. Box 105, Yusong, Daejon 305-353, South Korea*

Received 25 December 2001; accepted 4 December 2002

**Abstract**

The dislocation density and the composition of the β-Zr phase were determined using an X-ray diffractometer and TEM in an off-cut of the Zr–2.5Nb pressure tube irradiated in Wolsong Unit 1. Through Fourier analysis of diffraction line profiles of $\{1\,1\,\bar{2}\,0\}$, $\{1\,0\,\bar{1}\,0\}$ and $\{0\,0\,0\,1\}$ planes, an X-ray method determined the coherent block size and the lattice strain energy, from which the a- and c-type dislocation densities were evaluated assuming that the screw dislocation only contributes to the lattice strain energy. This X-ray method was demonstrated to reliably determine the a- and c-type dislocation densities in the Zr–2.5Nb tube which agreed well with the independently measured values for the same Zr–2.5Nb tube using the AECL's own method. For the first time, we developed a procedure to determine distributions of a- and c-type dislocation densities from distributions of the line broadening of the basal planes and the prism planes. Through this procedure, the volume-averaged c- and a-type dislocation densities in the Zr–2.5Nb were determined to be $2.69 \times 10^{14}$ m$^{-2}$ and $0.97 \times 10^{14}$ m$^{-2}$, respectively, which agree very well with those analyzed by TEM. The Nb content of the β-Zr phase was determined using an X-ray from a change in the lattice distance of the $\{1\,0\,0\}$ planes, which agrees well with that by the electron diffraction spectroscopy analysis on the extracted β-Zr particles.


*PACS:* 61.72.Ff

## 1. Introduction

Zr–2.5Nb pressure tubes are being degraded during operation in reactor, resulting in an increase in strength, a decrease in fracture toughness, irradiation growth and creep due to neutron irradiation [1,2]. Such irradiation embrittlement and a dimensional change of Zr–2.5Nb tubes are related to their microstructural change like a change in a- and c-type dislocation density and the phase decomposition of β-Zr particles [3]. Thus, to assess and predict the degradation of the Zr–2.5Nb tube with operational time, we need to keep track down a microstructural evolution of the Zr–2.5Nb tube. Since the microstructural evaluation of irradiated Zr–2.5Nb tubes using TEM takes a long time and has some risk of radiation exposure during the preparation of TEM samples, there is a need to set up another method like an X-ray method that easily can assess the microstructures of irradiated Zr–2.5Nb tubes with little radiation exposure. Therefore, the objective of this study is to analyze the dislocation density and the composition of the β-Zr phase in Zr–2.5Nb pressure tube with high confidence using a transmission electron microscope and an X-ray diffractometer. Griffiths reported an X-ray method for the microstructural evaluation of Zr–2.5Nb alloys 10 years ago, where the X-ray method underestimated the dislocation density compared to that by TEM in irradiated Zr–2.5Nb specimens [4].

Since the X-ray method yields different dislocation density with the orientation of the tube, a direct comparison of the X-ray method and the TEM method is

* Corresponding author. Tel.: +82-42 868 2359; fax: +82-42 868 8346.

*E-mail address:* yskim1@kaeri.re.kr (Y.S. Kim).

0022-3115/03/$ - see front matter 
doi:10.1016/S0022-3115(02)01694-X

not possible. It is because the TEM method produces a single representative value of dislocation density in the specimen regardless of the orientation. Therefore, this study is, for the first time, directed toward developing an X-ray method for determining a dislocation density distribution and the volume-averaged dislocation density in the Zr–2.5Nb tube. The feasibility of this method was demonstrated by comparing the dislocation density measured by a transmission electron microscope. In this study, the dislocation density was determined from coherent block sizes and lattice strain energies obtained through Fourier analyses of diffraction line profiles of α-Zr crystallographic planes. The Nb content of the β-Zr phase was also analyzed with the angle, $2\theta$ corresponding to the peak position of the $\{1\,0\,0\}$ planes and compared to the direct analysis of the extracted β-Zr particles using an electron diffraction spectroscopy.

## 2. Experimental procedures

### 2.1. Material

The specimens for the X-ray analysis were taken from the three sections of a Zr–2.5Nb pressure tube: the radial normal section (RS) plane, the tangential normal section (TS) plane and the longitudinal normal section (LS) plane as shown in Fig. 1. The examined tube is an off-cut ring of the Zr–2.5Nb tube irradiated to neutron fluences of $8.9 \times 10^{25}$ n/m$^2$ ($E > 1$ MeV) in the Wolsong Unit-1 nuclear power plant. To eliminate any effect of residual stress resulting from cutting and polishing, the specimens were pickled to remove the surface by more than 30 μm. The X-ray diffraction patterns were obtained using an X-ray diffractometer (Siemens D5000) with $CuK_\alpha$.

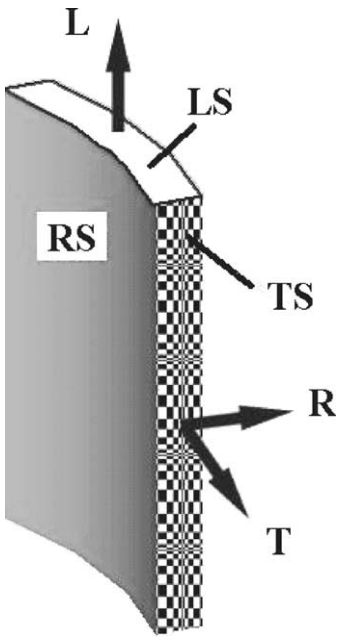


Fig. 1. Illustration of the L, T, R directions and LS, TS, RS planes defined herein.

Since the Zr–2.5Nb tube has a strong circumferential texture with a high fraction of $(0\,0\,0\,1)$ basal planes in the circumferential direction as shown in Fig. 2, the c-type dislocation density was determined from the TS and RS planes. Since the LS plane has a high fraction of $\{1\,0\,\bar{1}\,0\}$ planes in the longitudinal direction and the RS a high fraction of $\{1\,1\,\bar{2}\,0\}$ planes in the radial direction, the a-type dislocation density was determined from the LS and RS planes, respectively.

Thin foils of 0.1-mm-thick and 3 mm in diameter were cut out of the LS plane and electropolished in a solution of 10% perchloric acid and 90% ethanol at −35 °C using twin jet apparatus. TEM analyses were conducted using a JEOL-2000FX (200 keV) electron microscope. The dislocation density was determined by a line intercept method where the number of the intersections between concentric circles and dislocations were counted:

$$\rho = \frac{2N}{Lt}, \tag{1}$$

where $\rho$ is the dislocation density, $N$ is the number of the intersections of dislocations, $L$ is a secant circle length and $t$ is a foil thickness.

### 2.2. Coherent block size and the lattice strain energy

Broadening of X-ray diffraction lines is determined by the sizes of coherent blocks with the perfect crystalline lattice and lattice strain energies at the lattice distorted region between the coherent blocks [5,6]. Thus, the line broadening becomes larger with a decrease in the coherent block size and an increase in the lattice strain energy. When the coherent block size increases to more than 200 nm, the line broadening becomes independent of the coherent block size irrespective of the reflection order, thus separating the effect of the coherent block size from the effect of the lattice strain energy [6]. Further, the $CuK_\alpha$ line was separated from the superposed diffraction lines using Gangulee's method [7]. The real line broadening was determined after applying a pseudo-Voigt approximation to compensate an error from the X-ray machine [8]. The line broadening from fully recrystallized zirconium iodide was taken as a standard for the correction of the instrumental broadening. The line shape analysis as outlined by [9,10] was adopted for the quantitative determination of coherent block sizes and lattice strain energies. When the line profile is described as a Fourier series, the coefficient of

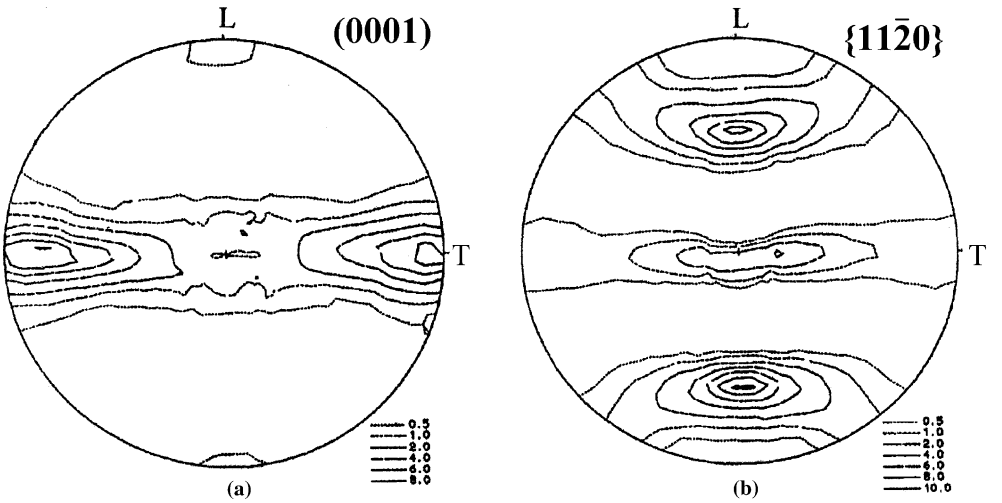


Fig. 2. Direct pole figures of (a) (0 0 0 1) and (b) (1 1 $\bar{2}$ 0) planes in the Wolsong Zr–2.5Nb tube.

the symmetrical Fourier series corresponds to the product of the coefficients of the coherent block size and the lattice strain energy [9,10]:

$$A_n = A_n^S A_n^D(l), \tag{2}$$

where $A_n$ is the Fourier coefficient, $A_n^S$ is the coefficient of the coherent block size, $A_n^D$, the coefficient of the lattice strain energy, is equal to $\exp(-2\pi^2 l^2 n^2 \varepsilon_n^2)$, $l$ is the reflection order of a diffraction plane, for example, (0 0 0 1), $n$ is an integer constant, $\varepsilon_n$ is the lattice strain energy. When a log plot of Fourier coefficients is made against $l^2$ the intercept and slope of this plot yield $A_n^S$ and $A_n^D$ or $\varepsilon_n$ as shown in Fig. 3 [11]. By plotting $A_L^S$ and $\varepsilon_L$ as a function of $L$ (Fig. 4) where $L = n\Delta L = n\lambda/\{2(\sin\theta_1 - \sin\theta_2)\}$, $\theta_1$, $\theta_2$ are the boundary angles of the line profile described as a Fourier series, the coherent block size is set as the intersection with the $L$-axis when a tangent line is drawn to the curve of $A_L^S$ [9]:

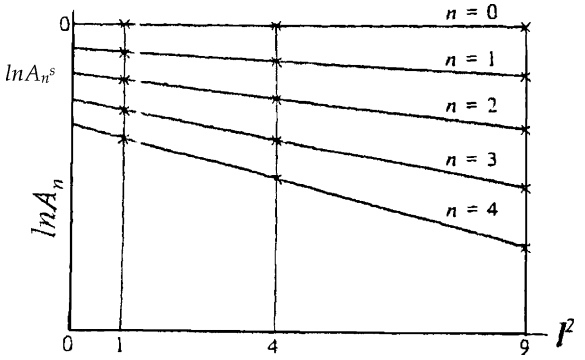


Fig. 3. Logarithmic plot to separate the effects of the coherent block size and lattice strain energy with multiple reflection orders (0 0 0 1) [10].

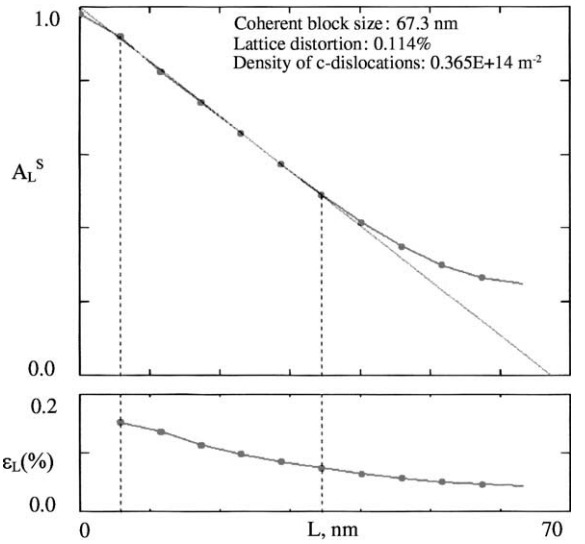


Fig. 4. Dependence of the Fourier coefficient and the lattice strain energy on $L$.

$$(\mathrm{d}A_L^S/\mathrm{d}L)_{L\to 0} = -1/D, \tag{3}$$

where $D$ is the coherent block size. It is to be noted that the tangent line is optimized to yield a minimal mean square error in the least square method in drawing a straight line from the $A_L^S$ values. Since $\varepsilon_L$ varies with $L$ as shown in Fig. 4, it is hard to choose the right value of $\varepsilon_L$. Thus, we set the lattice strain energy to become an average value of $\varepsilon_L$ over the $L$ used in drawing the optimized tangent line than to determine $\varepsilon_L$ at an arbitrary $L$ (Fig. 4). This method is unique against the method for the determination of lattice strain energy reported by others [4,10,12].

Table 1
Comparison of the measured dislocation density in the Zr–2.5Nb pressure tube

| Participants | Section plane | RS ($\times 10^{14}/m^2$) | TS ($\times 10^{14}/m^2$) | LS ($\times 10^{14}/m^2$) |
|---|---|---|---|---|
| This study | a-type dislocation | 1.28 | – | 3.05 |
| | c-type dislocation | 0.43 | 1.00 | |
| AECL | a-type dislocation | 1.44 | – | 3.13 |
| | c-type dislocation | 0.3 | 0.66 | – |

### 2.3. Determination of dislocation density

The dislocation density, $\rho$, can be obtained by relating the energies of dislocations, $vF$ with the total strain energy, $V$ [4,13]:

$$\text{the dislocation density,} \quad \rho = V/(vF) \cong \frac{6\pi A\varepsilon^2}{FGb^2 \ln\left(\frac{D}{2r_0}\right)} = \frac{K\varepsilon^2}{b^2 \ln\left(\frac{D}{2r_0}\right)}, \tag{4}$$

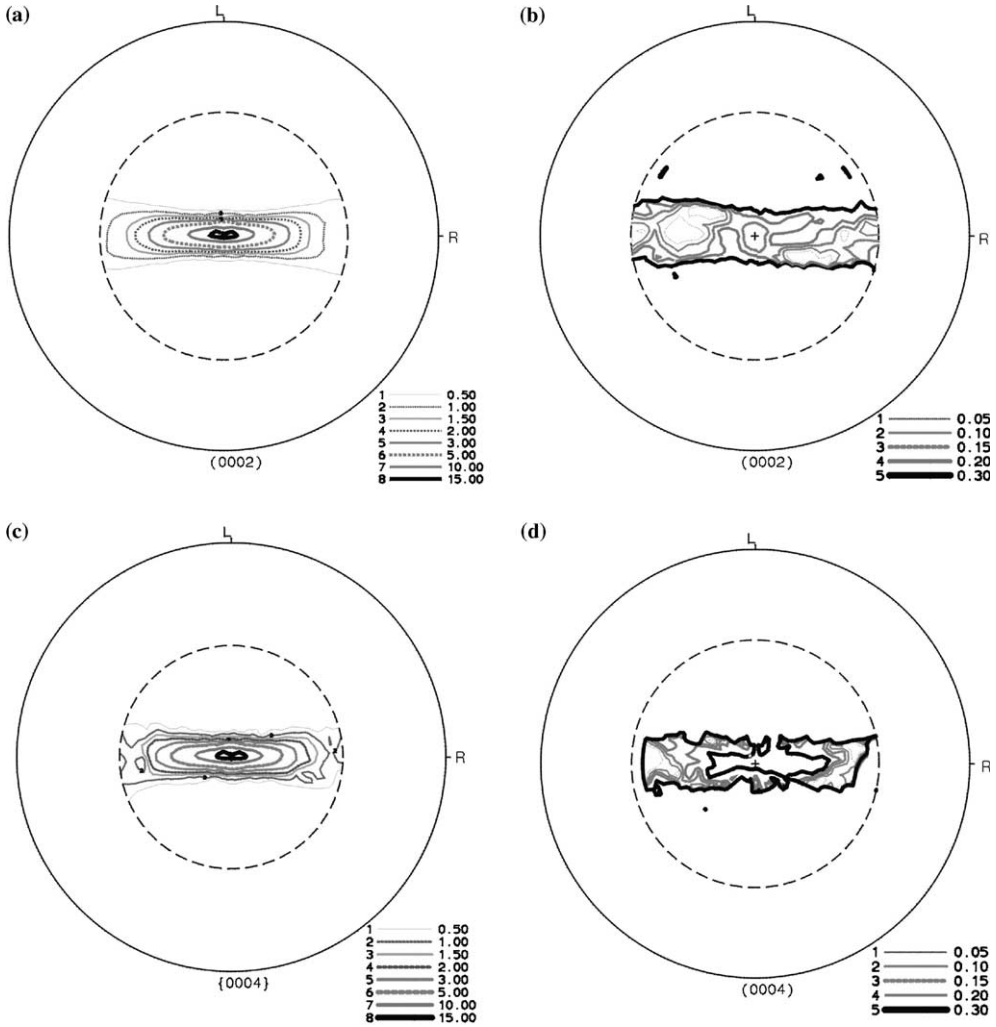


Fig. 5. (a) Incomplete (0 0 0 2) pole figures, (b) the distribution of the (0 0 0 2) line broadening, (c) incomplete (0 0 0 4) pole figures and (d) the distribution of the (0 0 0 4) line broadening for the TS plane of the Zr–2.5Nb tube.

where the total lattice energy, $V$, is $3AE(\varepsilon^2)/2$ and the energy of a screw dislocation, $v$ is $Gb^2\ln(r/r_0)/4\pi$, $F$ is a factor representing interactions between dislocations, $E$ and $G$ are Young's and shear moduli, $\varepsilon$ and $D$ are the lattice strain energy and the coherent block size determined by X-ray, $b$ is Burgers' vector, $r$ and $r_0$ are the radius and core radius of the dislocation and $A$, $K$ are the constants. The density of a- and c-type dislocations is obtained as such:

$$\rho_a = \frac{K_a\varepsilon_a^2}{b_a^2}\frac{1}{\ln(D_0/2r_0)}, \quad \rho_c = \frac{K_c\varepsilon_c^2}{b_c^2}\frac{1}{\ln(D_0/2r_0)}, \tag{5}$$

where $b_a$ and $b_c$ are Burgers vectors corresponding to $1/3\langle 11\bar{2}0\rangle$ and [0001], respectively, $r_0 = 1$ nm, $K_a$, $K_c$ are the constants corresponding to 52.1 and 26, respectively [4].

## 3. Results and discussion

### 3.1. Dislocation density of the Zr–2.5Nb tube

The Wolsong Zr–2.5Nb tube has a strong circumferential texture with the greater part of the (0001) poles oriented in the circumferential direction and the less part of the (0001) poles in the radial direction as shown in Fig. 2. Thus, the c-type dislocation density was evaluated from the line broadening of the {0001} planes on the TS and RS sections as shown in Fig. 4. In contrast, the a-type dislocation density was determined from the line broadening of the $\{10\bar{1}0\}$ planes on the LS section and that of the $\{11\bar{2}0\}$ planes on the RS section. Table 1 shows the density of a- and c-type dislocations in the Zr–2.5Nb tube measured by the X-ray

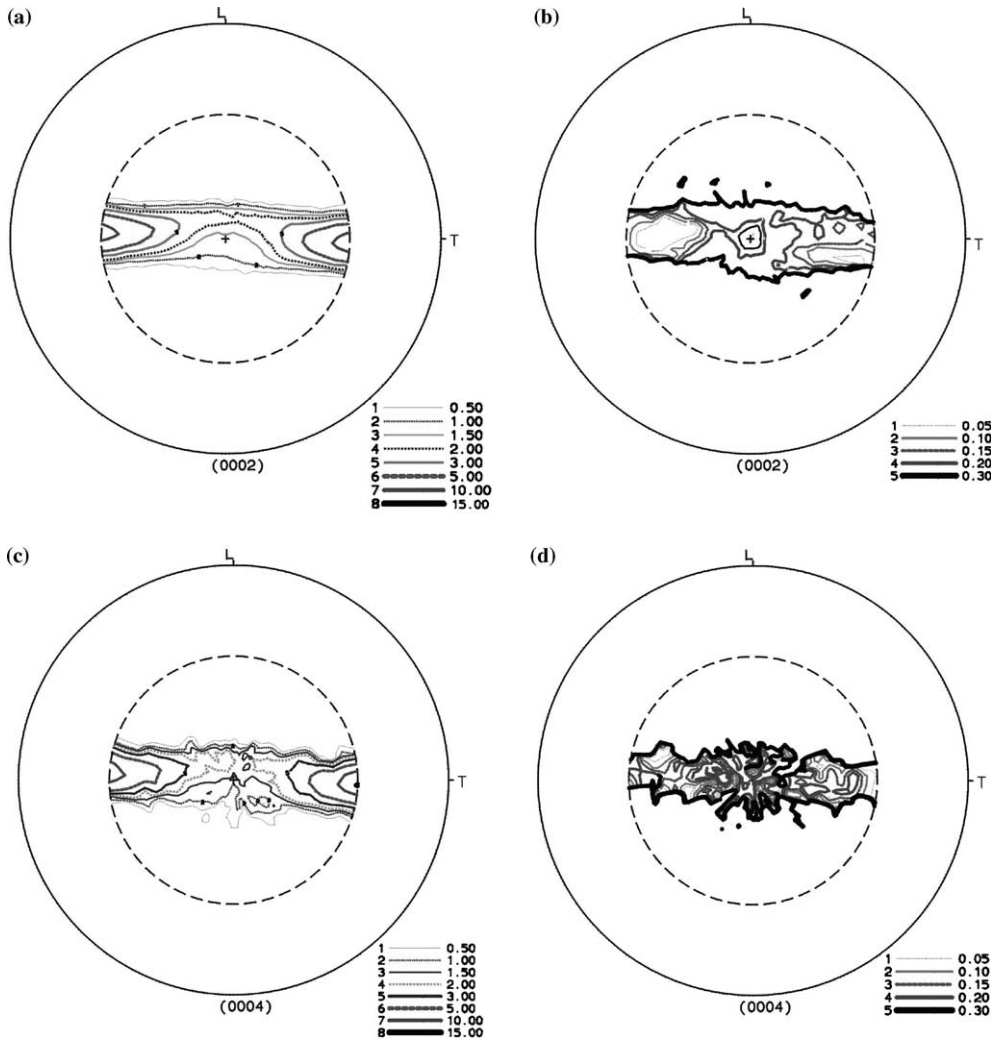


Fig. 6. (a) Incomplete (0002) pole figures, (b) the distribution of the (0002) line broadening, (c) incomplete (0004) pole figures and (d) the distribution of the (0004) line broadening for the RS plane of the Zr–2.5Nb tube.

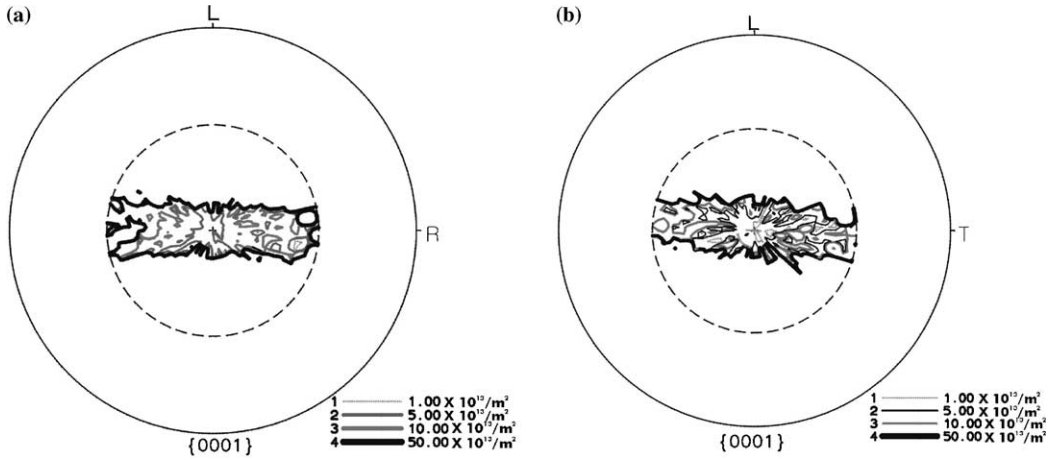


Fig. 7. Incomplete distribution of the density of c-dislocations with the tilt angles of up to 55° for (a) the RS and (b) TS planes of the Zr–2.5Nb tube.

method. To demonstrate that the measured densities of a- and c-type dislocation by this method are accurate, we had the same specimen subjected to an X-ray analysis by AECL whose detailed method was described elsewhere [14]. As shown in Table 1, the X-ray method developed in this study yields similar dislocation densities to those determined independently by AECL [15]. Therefore, our X-ray method is concluded to be very reliable and comparable to the AECL's method.

### 3.2. Distribution of the dislocation density in a Zr–2.5Nb tube

The dislocation density determined by the X-ray method cannot be directly compared to that by TEM because the former varies with the tube sections but the latter is a volume average value irrespective of the tube orientation. For the first time, this study developed a procedure to assess a distribution of the dislocation density in the Zr–2.5Nb tube. Like a procedure to determine texture, distributions of the line broadening of the basal plane and the prism plane were determined by changing the tilting angle $\psi$ from 0° to 70° and the rotation angle from 0° to 360°. It is kept in mind that the real line broadening is calibrated against the line broadening obtained experimentally from a fully recrystallized zirconium iodide that was made by annealing at 850 °C for 48 h in a vacuum of more than $5 \times 10^{-5}$ Torr. As a result of that, the distributions of a- or c-type dislocation densities were obtained using Eq. (5) from the distributions of coherent block size and the lattice strain energy determined from those of the line broadening of the prism planes or the basal planes. Thus, all the dislocation densities can be displayed as a distribution curve in the stereographic projection of a sample.

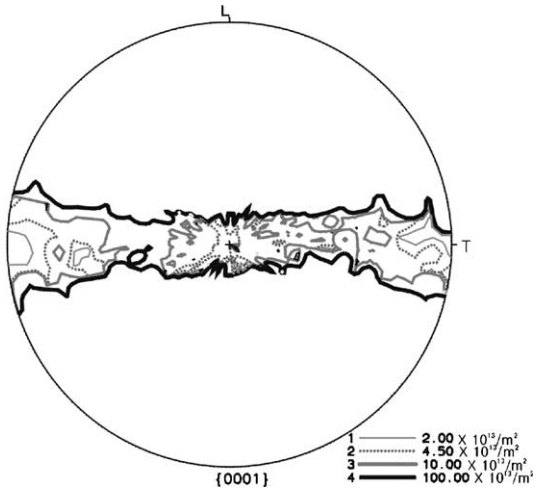


Fig. 8. Complete distribution of the density of c-type dislocations with the center of the pole figure corresponding to the transverse direction of the Zr–2.5Nb tube.

However, the distribution of c-type dislocation density determined either from the RS or the TS specimen does not cover part of the specimen with the tilting angle ranging from 70° to 90°. Thus, a fitting procedure was applied to get a complete dislocation density $V(\rho_c)$ where the dislocation density distribution at the tilt angles ranging from 0° to 50° or 60° was obtained from the TS specimen only and the dislocation density distribution at the tilt angles more than that was obtained by superposing and mutually leveling the dislocation density distributions of the RS and TS specimens [16]. In contrast, the complete distribution of a-type dislocation density was made only from the LS specimen with the tilt angles of up to 35° because the maximum of the

$\{1\,0\,\bar{1}\,0\}$ poles converges on the longitudinal direction of this tube.

*3.2.1. Conditions for the calculation of dislocation density*

When the intensity of X-ray lines is low and their broadening is large as in the texture minima, the rational parameters of the approximate function cannot be found. Further, for an annealed specimen, the Fourier analysis involves significant errors due to the small physical broadening of X-ray lines even with reasonable approximate function parameters. Thus, we set the following conditions in the procedure for a calculation of the dislocation density:

(1) Dislocation density is assumed to be $1 \times 10^{16}$ m$^{-2}$ at the maximum when the calibrated line profiles meet one of the following conditions: (a) $I - I_S \leqslant 0$, (b) $B - B_S \leqslant 0$, (c) the fraction of the Gauss component in the approximation function, $f$, is out of the interval between 0 and 1 or (d) the approximation by a pseudo-Voigt function yields more than 60% error, where $I$ and $I_S$ are the line intensity for the specimen and the standard, respectively, $B$ and $B_S$ are the line broadening for the specimen and the standard.

(2) When the Fourier analysis fails due to the mutual incompatibility of the parameters for the approximation of the lines even with all reasonable input parameters and the approximation error of less than 60%, the dislocation density is assumed to be $1 \times 10^{12}$ m$^{-2}$ at the minimum.

As a result, the dislocation density within texture minima is maximal. These prescriptions are based on the concept on the substructure inhomogeneity of textured

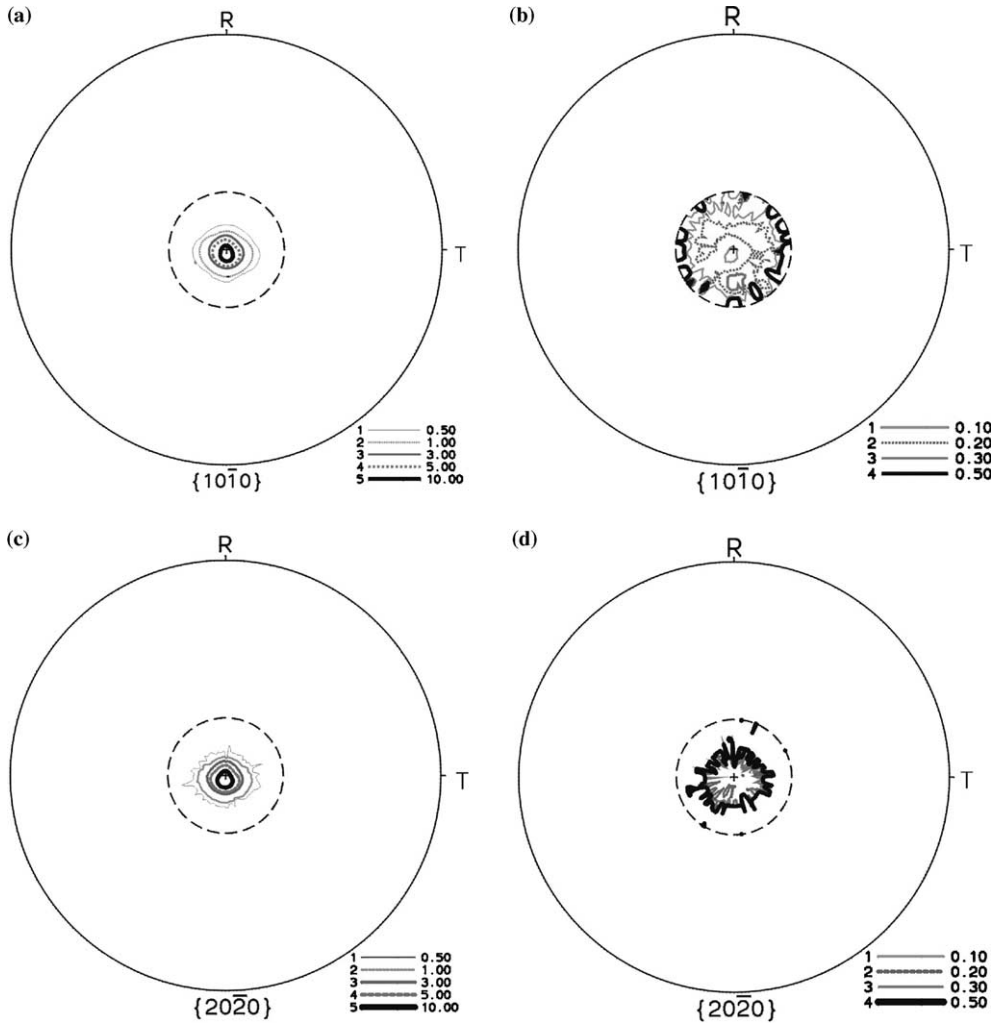


Fig. 9. (a) Complete $\{1\,0\,\bar{1}\,0\}$ pole figures, (b) the distribution of the $(1\,0\,\bar{1}\,0)$ line broadening, (c) complete $(2\,0\,\bar{2}\,0)$ pole figures and (d) the distribution of the $(2\,0\,\bar{2}\,0)$ line broadening for the LS plane of the Zr–2.5Nb tube.

metal materials [8,16]. At the texture minimum, the size of coherent blocks decreases and the lattice distortion increases. This is quite understandable by considering the conditions at grain boundaries with orientations of texture maxima and minima. Since the dislocation density depends on the block size and lattice strain, we assume that the maximum attainable dislocation density is $1 \times 10^{16}$ m$^{-2}$ in the most disperse fraction of our textured specimen. When the program fails due to an acceptable ratio of line widths of the sample and the standard, we consider reflecting grains as almost perfect with the dislocation density of as low as $1 \times 10^{12}$ m$^{-2}$.

*3.2.2. Distributions of a- and c-type dislocation density*

Fig. 5 shows incomplete line broadening distributions of (0 0 0 2) and (0 0 0 4) planes obtained from the {0 0 0 2} basal pole figures for the TS specimen while Fig. 6 shows these for the RS specimen. Here, the incomplete line broadening distributions represent those obtained at the tilt angles ranging from 0° to 55°. Based on these line broadening distributions as shown in Figs. 5 and 6, incomplete distributions of dislocation density were made from each specimen as shown in Fig. 7. By combining two incomplete distributions of c-type dislocation density through the fitting procedure described above, we made a complete distribution of c-type dislocation density as shown in Fig. 8. Using incomplete broadening distributions of the $(1\,0\,\bar{1}\,0)$ and $(2\,0\,\bar{2}\,0)$ lines obtained from the incomplete $(1\,0\,\bar{1}\,0)$ and $(2\,0\,\bar{2}\,0)$ pole figures (Fig. 9), likewise, the complete distributions of a-type dislocation density were obtained as shown in Fig. 10. It should be noted that the highest density of a- and c-type dislocations occurs at some angles away from the longitudinal or transverse directions, respectively, corresponding to the highest pole density, or texture maxima of $(1\,0\,\bar{1}\,0)$ or (0 0 0 1) planes.

A correlation between complete dislocation density (Figs. 8 and 10) and pole density was constructed as shown in Fig. 11, by making point-by-point comparisons between them. The largest scatter of dislocation density corresponded to the lowest pole density while the low scatter of dislocation density was always observed at the highest pole density. These results look quite reasonable because the grains in the texture minima or the lowest pole density have diverse orientations and

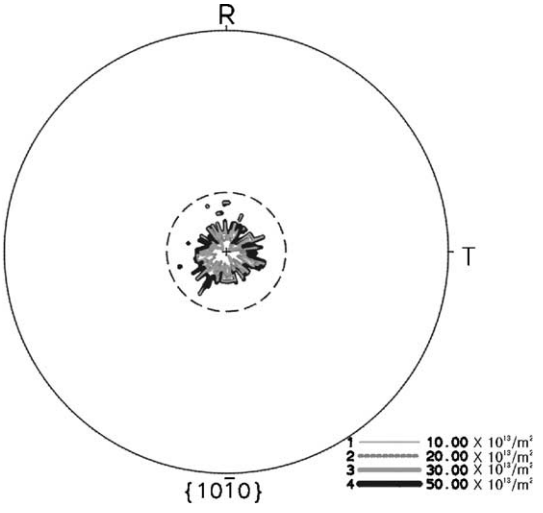


Fig. 10. Complete distribution of the a-type dislocation density with the pole figure center corresponding to the longitudinal direction of the Zr–2.5Nb tube.

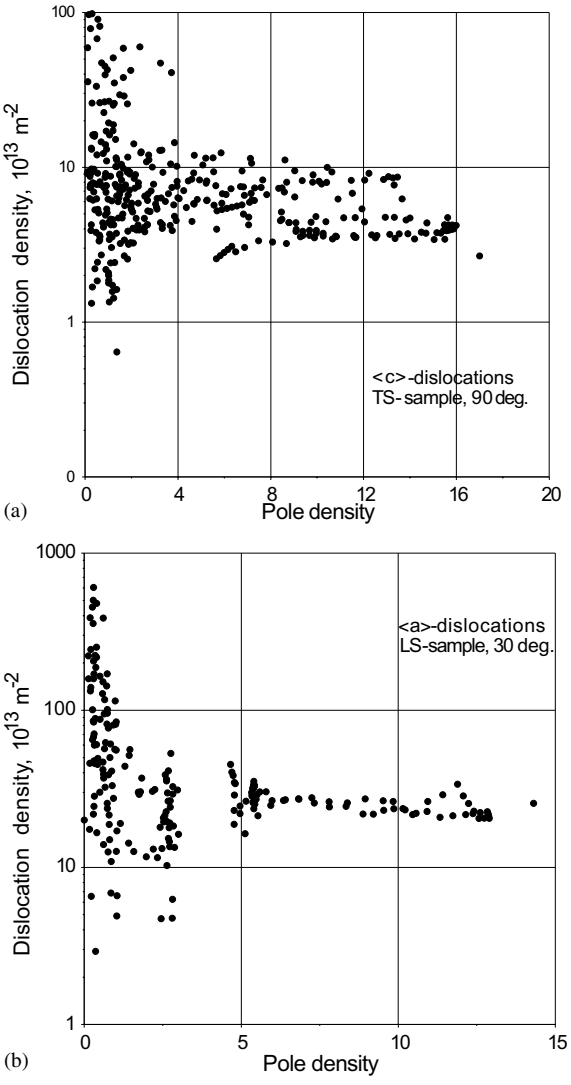


Fig. 11. Correlation between dislocation density and pole density from (a) complete {0 0 0 1} pole figures for the TS of the Zr–2.5Nb tube and from (b) complete $\{1\,0\,\bar{1}\,0\}$ pole figures for the LS plane where 90° and 30° mean the maximum tilt angle for the TS and LS samples, respectively.

distorted crystalline lattice and the grains in the texture maxima or the highest pole density have more perfect lattice [17]. Fig. 12 shows the volume fractions of c-type dislocation density for incomplete (0 0 0 1) pole figures from TS and RS specimens while Fig. 13 shows the volume fractions of c-type dislocation density for complete (0 0 0 1) pole figures. Likewise, the distributions of volume fractions of a-type dislocation density were also made as shown in Fig. 14. The mean values of a- and c-type dislocation density, $\rho_{mean}$ were $2.69 \times 10^{14}$ $m^{-2}$ and $0.97 \times 10^{14}$ $m^{-2}$, respectively. One thing to note is that the most probable dislocation density does not coincide with its mean value, suggesting that the high dislocation density of low volume fraction seems to contribute significantly to the mean dislocation density.

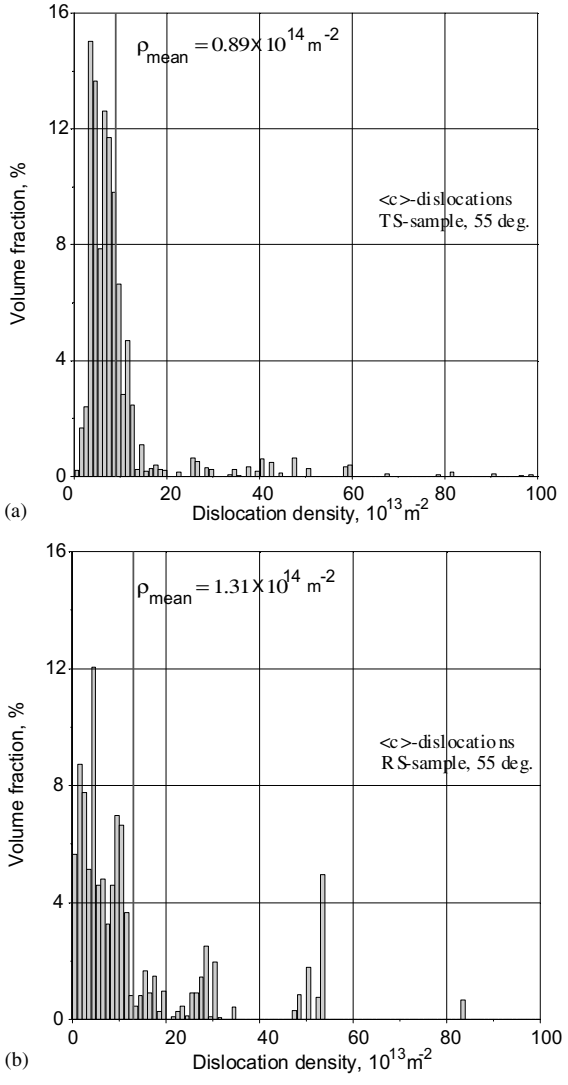


Fig. 12. Incomplete distribution of c-type dislocation density obtained from incomplete (0 0 0 1) pole figures for the TS and RS planes of the Zr–2.5Nb tube with the tilt angles of up to 55°.

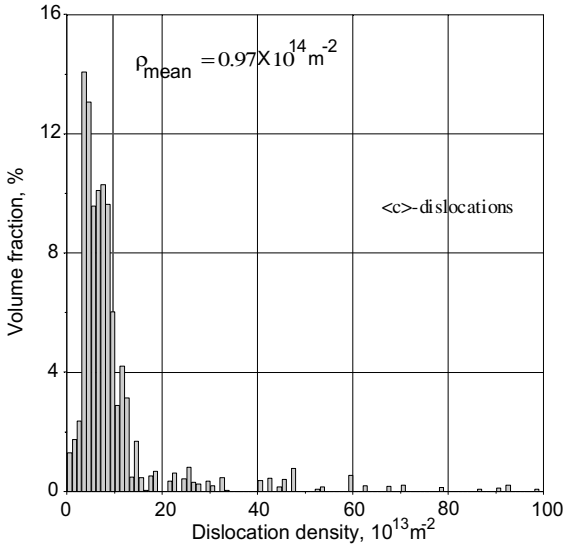


Fig. 13. Complete distributions of c-type dislocation density for the Zr–2.5Nb tube.

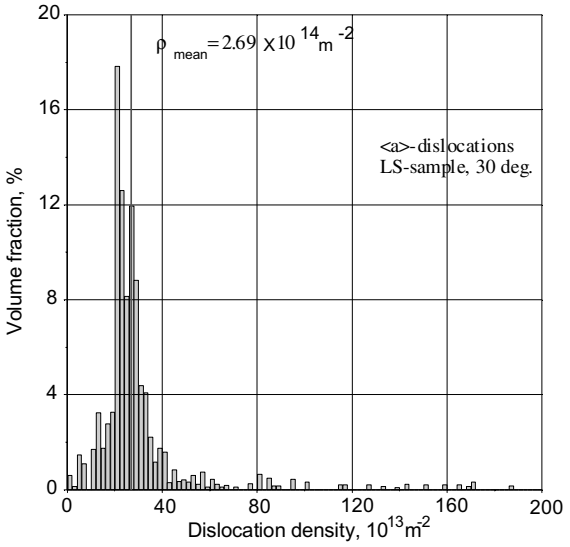


Fig. 14. Complete distribution of a-type dislocation density for the Zr–2.5Nb tube obtained with the tilt angles of 30°.

### 3.3. Comparison of the dislocation density determined by TEM and the X-ray method

To verify the feasibility of the X-ray method, the same specimen was subjected to an analysis of dislocation densities using a transmission electron microscope.

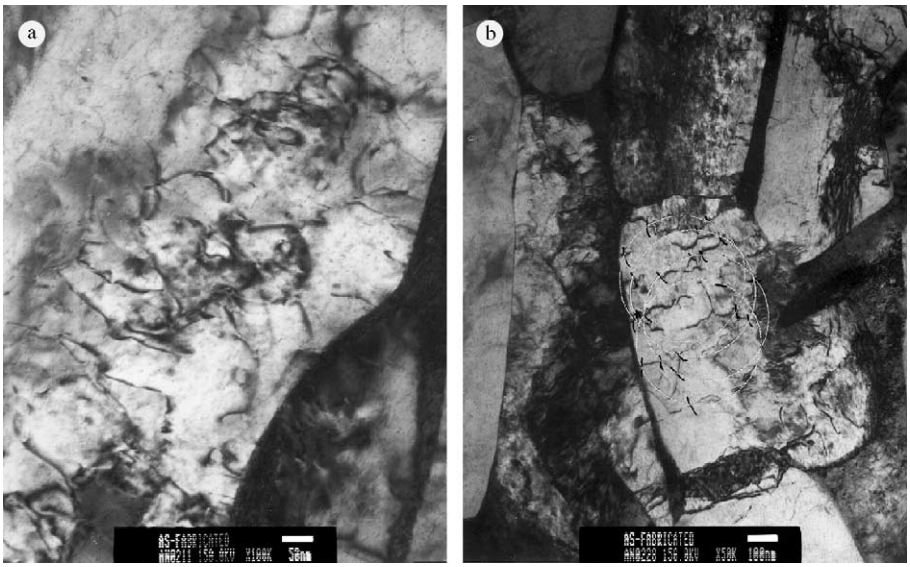


Fig. 15. Observation of (a) a-type dislocations and (b) c-type dislocations in the Zr–2.5Nb pressure tube using TEM.

Fig. 15 shows typical distribution of a- and c-type dislocations in the Zr–2.5Nb tube whose dislocation densities have been already known by the X-ray method. The densities of a- and c-type dislocations were determined using a line intercept method to be $4.0 \times 10^{14}$ $m^{-2}$ and $0.97 \times 10^{14}$ $m^{-2}$. Surprisingly, these values agree excellently with those determined by the volume fraction distribution of dislocation density as shown in Figs. 13 and 14. Thus, it is concluded that the X-ray method involving the method to find out the dislocation density distribution is quite feasible and reliable in determining the volume-averaged dislocation density in Zr–2.5Nb pressure tubes.

### 3.4. Analysis of the Nb content in the β-Zr phase

One of the microstructural changes the Zr–2.5Nb pressure tube has undergone with their operational time is the transformation of the β-Zr phase into the β-Nb phase. Since this decomposition behavior of the β-Zr phase can affect hydrogen pickup rate and creep of the Zr–2.5Nb tube [18,19], it is very important to accurately and reliably evaluate the composition of the β-Zr phase. In this study, the composition of the β-Zr phase is determined from the Vegard's rule [20] by investigating the angular position of X-ray lines for the β-Zr phase. However, the determination of the angular position of the lines is complicated because, firstly, the volume fraction of the β-Zr phase is relatively low, resulting in low line intensity, secondly, the localized reflection lines due to a texture of the β-Zr phase and lastly, overlapping of X-ray lines of α-Zr, β-Zr, ω-phase. Thus, we developed an optimized procedure where the higher intensity of the (2 0 0) line of the β-Zr phase can be obtained separately by subjecting the RS specimen to X-ray diffraction analysis only in the angular range from 52° to 56°.

Fig. 16 shows the (0 0 2) lines of the β-Zr for the respective RS plane of the Zr–2.5Nb specimen and the

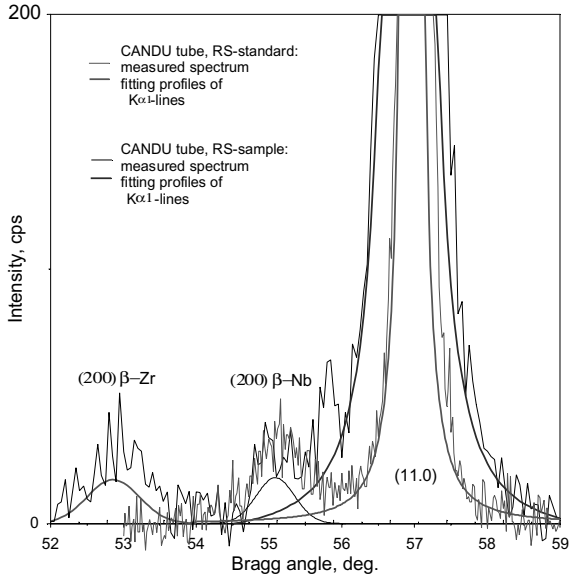


Fig. 16. Optimal range of the diffraction spectrum for the determination of the Nb concentration in the β-Zr phase that were taken from the RS sample and standard of the Zr–2.5Nb tube. Here, the RS standard represents the fully annealed Zr–2.5Nb at 530 °C for 15 h.

fully annealed Zr–2.5Nb tube at 580 °C for 15 h (the RS standard). From the angular positions for both of the specimens in the range from 52° to 56°, the Nb contents were determined using a plot shown in Fig. 17 [20]. The Nb content of the β-Zr phase was 43 at.% for the Zr–2.5Nb tube and increased to 88 at.% for the annealed Zr–2.5Nb tube, which agrees with the β-Nb composition [21]. To verify the feasibility of the X-ray method, the Nb content of the β-Zr phase also was determined using TEM in two ways. Firstly, the lattice constants of (1 1 0) planes were obtained from the selected area diffraction pattern (SADP) using the following relationship [22]:

$d_{(1\,1\,0)} = d_{(0\,0\,0\,1)}R/r$, where $d_{(1\,1\,0)}$ and $d_{(0\,0\,0\,1)}$ are the respective lattice spacing of (1 1 0) and (0 0 0 2) planes, $R$ and $r$ are the radius of the first ring of the diffracted

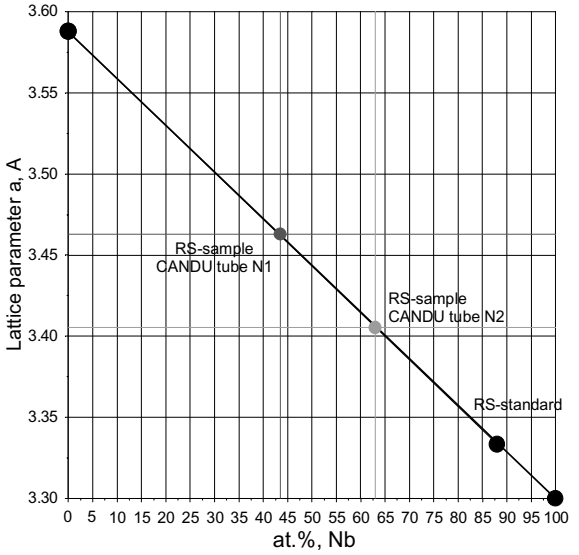


Fig. 17. Dependence of the lattice distance, $d_{100}$ on the Nb content in the β-Zr phase. CANDU tubes N1 and N2 represents the unirradiated Wolsong 1 Zr–2.5Nb tube and a quad-melted Zr–2.5Nb tube, respectively while the RS-standard means the fully annealed Zr–2.5Nb tube at 530 °C for 15 h.

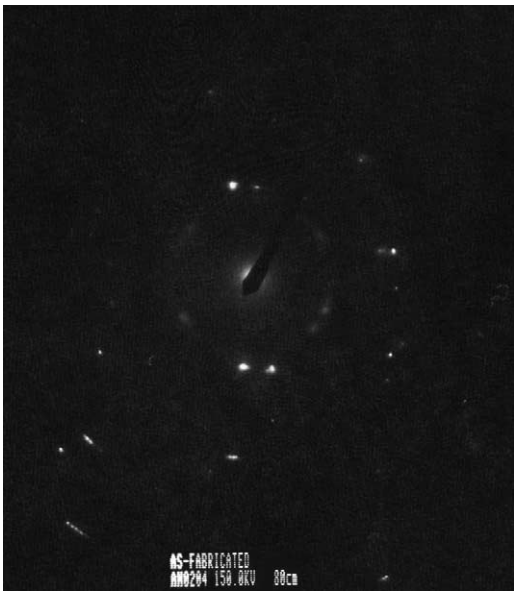


Fig. 18. Selected area diffraction pattern of the α-Zr and β-Zr phases of the Zr–2.5Nb pressure tube.

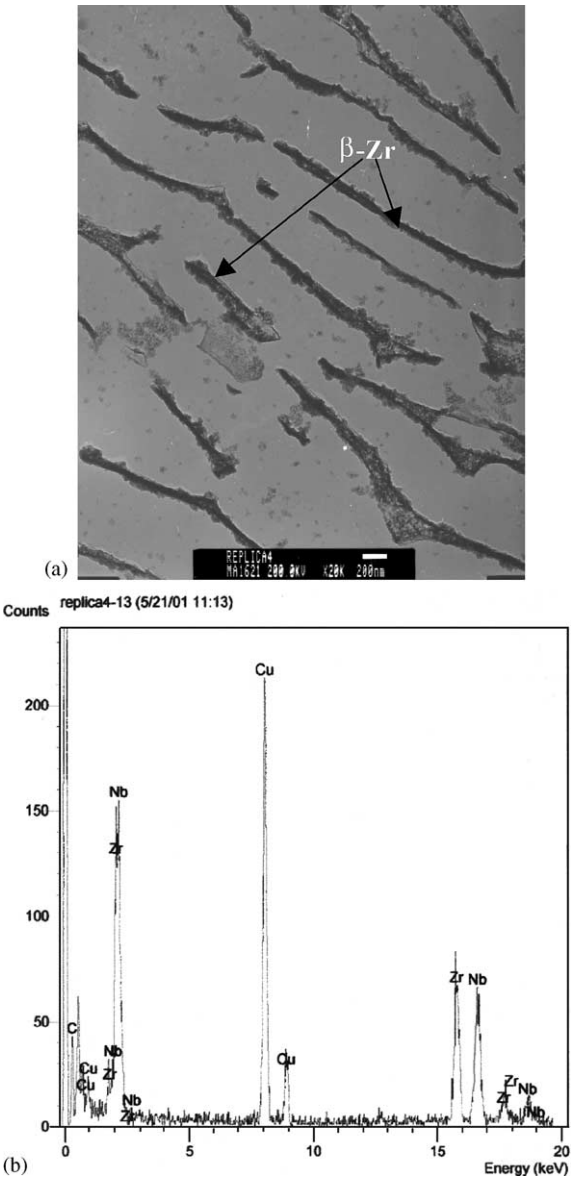


Fig. 19. Micrograph of the β-Zr phase extracted from Zr–2.5Nb pressure tube by a carbon replica film (a) and the EDX analysis of the extracted β-Zr phase.

Table 2
The Nb content in the β-Zr phase determined by X-ray and TEM

| Testing method | X-ray (at.%) | | TEM (at.%) | |
|---|---|---|---|---|
| | This study | AECL | SADP | EDX |
| Nb content in β-Zr phase | 43 | 67 | 38 | 44 |

beam of α-Zr and β-Zr as shown in Fig. 18. The Nb content of the β-Zr phase was determined using a relationship between the lattice constant and the Nb content [20]. Secondly, the β-Zr particles were extracted by a carbon replica method as shown in Fig. 19 and were subjected to electron diffraction spectroscope (EDS) analysis. Table 2 summarizes the Nb contents determined with the X-ray method, the EDS analysis on the extracted β-Zr particles and the SADP method along with the AECL's own X-ray method where the Nb content was determined using β(2 0 0) reflections [2,15]. Considering that the EDS analysis on the extracted β-Zr phase yields the most accurate Nb content, the X-ray method developed by this study surprisingly determined the same Nb content as the EDS analysis on the extracted β-Zr phase did. In contrast, the SADP method slightly underestimated the Nb content while the AECL's X-ray method overestimated it considerably. Thus, it is concluded that our X-ray method is accurate and reliable in determining the Nb content, where the (1 0 0) line is selectively analyzed on the radial normal section of the Zr–2.5Nb tube.

## 4. Conclusion

We developed an X-ray method to determine a- and c-type dislocation densities from the coherent block size and the lattice strain energy obtained through the Fourier analysis of diffraction line profiles of $\{1\,1\,\bar{2}\,0\}$, $\{1\,0\,\bar{1}\,0\}$ and $\{0\,0\,0\,1\}$ planes. The a- and c-type dislocation densities of the Zr–2.5Nb tube were analysed with this method, the result of which agree quite excellently with those determined independently by the AECL's own method. This method, however, yields a different dislocation density with the orientation of the tube. For the first time, we developed a procedure to evaluate a distribution of the dislocation density in the Zr–2.5Nb tube, where distributions of the line broadening of the basal plane and the prism plane were determined by changing the tilting angle $\psi$ from 0 to 70 or less degrees and the rotation angle from 0° to 360°. The complete c-type dislocation density were made by combining its distributions obtained from the radial normal section plane and transverse normal section plane with a fitting procedure while the complete a-type dislocation density was made only from the longitudinal normal section plane. The dislocation density distribution method yields average values of a- and c-type dislocation densities of the Zr–2.5Nb tube to be $2.69 \times 10^{14}$ m$^{-2}$ and $0.97 \times 10^{14}$ m$^{-2}$, which is quite comparable to those by a linear intercept method using TEM. It is concluded that the X-ray method is quite feasible and reliable in determining the dislocation density in Zr–2.5Nb pressure tubes.

The composition of the β-Zr phase was analyzed using an X-ray method where the lattice distance of {0 0 1} planes was determined from the angular position of the β {0 0 1} lines. This method determined the Nb content of the β-Zr in the Zr–2.5Nb to be 43 at.%, which agrees quite well with that determined by the EDS analysis on the extracted particles with a carbon replica method. Therefore, the X-ray method is concluded to reliably and accurately determine the Nb content of the β-Zr phase in Zr–2.5Nb pressure tubes.

## Acknowledgements

This work has been carried out as part of the Nuclear R&D program supported by the Ministry of Science and Technology in Korea. One of the authors would like to express sincere thanks to Y. Perlovich and M. Isaenkova for their X-ray analysis and to A. Tselishchev for TEM analysis.

## References

[1] C.K. Chow, C.E. Coleman, M.H. Koike, A.R. Causey, C.E. Ells, R.R. Hosbons, S. Sagat, V.F. Urbanic, D.K. Rodgers, Zirconium in the Nuclear Industry: Eleventh International Symposium, ASTM STP, vol. 1295, 1996, p. 469.
[2] R.R. Hosbons, P.H. Davies, M. Griffiths, S. Sagat, C.E. Coleman, Zirconium in the Nuclear Industry: Twelfth International Symposium, ASTM STP, vol. 1354, 2000, p. 122.
[3] M. Griffiths, J.F. Mecke, J.E. Winegar, Zirconium in the Nuclear Industry: Eleventh International Symposium, ASTM STP, vol. 1295, 1996, p. 580.
[4] M. Griffiths, J.E. Winegar, J.F. Mecke, R.A. Holt, Adv. X-ray Anal. 35 (1992) 593.
[5] P. Gay, P.B. Hirsh, A. Kelly, Acta Met. 1 (1953) 315.
[6] A. Taylor, X-ray Metallography, John Wiley, New York, 1961, p. 687.
[7] A. Gangulee, J. Appl. Cryst. 3 (1970) 272.
[8] Y. Perlovich, H.J. Bunge, M. Isaenkova, Textures Microstruct. 29 (1997) 241.
[9] B.E. Warren, Progr. Met. Phys. 8 (1959) 147.
[10] S.K. Chatterjee, S.P. Sen Gupta, J. Mater. Sci. 9 (1974) 953.

[11] Y.S. Kim, KAERI Technical Report, KAERI-TR-1672/2000.
[12] S.K. Chatterjee, S.P. Sen Gupta, J. Mater. Sci. 10 (1975) 1093.
[13] G.K. Williamson, R.E. Smallman, Philos. Mag. 1 (1956) 34.
[14] M. Griffiths, D. Sage, R.A. Holt, C.N. Tome, Metall. Mater. Trans. 33A (2002) 859.
[15] S.S. Kim, Y.S. Kim, J. Kor. Nucl. Soc. 32 (2000) 1.
[16] Y. Perlovich, H.J. Bunge, M. Isaenkova, Zeitschrift fur Metallkunde 91 (2000) 149.
[17] Y. Perlovich, H.J. Bunge, V. Fresno, M. Isaenkova, N.J. Park, L. Wcislak, M. Zuev, J. De Physique IV, Collogue C1, 6 (1996) 149.
[18] Y.S. Kim, Y.C. Suh, S.B. Ahn, Y.M. Cheong, K.S. Im, Korean Society of Mechanical Engineering, Proceeding of Symposium on 1st Material and Fracture, 2001, p. 185.
[19] V.F. Urbanic, M. Griffiths, Zirconium in the Nuclear Industry: Twelfth International Symposium, ASTM STP, vol. 1354, 2000, p. 641.
[20] G.B. Grad, J.J. Pieres, A.F. Guillermet, G.J. Cuello, R.E. Mayer, J.R. Granada, Zeitschrift fur Metallkunde 86 (1995) 395.
[21] C.E. Lundin, R.H. Cox, USAEC Report, GEAP-4089, 1962.
[22] Young Suk Kim, KAERI Technical Report, KAERI-TR-1490/2000, KAERI, 2000.